Published OnlineFirst March 27, 2018; DOI: 10.1158/1535-7163.MCT-17-1077

Large Molecule Therapeutics

Molecular Cancer Therapeutics

IMGN779, a Novel CD33-Targeting Antibody–Drug Conjugate with DNA-Alkylating Activity, Exhibits Potent Antitumor Activity in Models of AML

Yelena Kovtun[1], Paul Noordhuis[2], Kathleen R. Whiteman[1], Krystal Watkins[1], Gregory E. Jones[1], Lauren Harvey[1], Katharine C. Lai[1], Scott Portwood[3], Sharlene Adams[1], Callum M. Sloss[1], Gerrit Jan Schuurhuis[2], Gert Ossenkoppele[2], Eunice S. Wang[3], and Jan Pinkas[1]

Abstract

The myeloid differentiation antigen CD33 has long been exploited as a target for antibody-based therapeutic approaches in acute myeloid leukemia (AML). Validation of this strategy was provided with the approval of the CD33-targeting antibody–drug conjugate (ADC) gemtuzumab ozogamicin in 2000; the clinical utility of this agent, however, has been hampered by safety concerns. Thus, the full potential of CD33-directed therapy in AML remains to be realized, and considerable interest exists in the design and development of more effective ADCs that confer high therapeutic indices and favorable tolerability profiles. Here, we describe the preclinical characterization of a novel CD33-targeting ADC, IMGN779, which utilizes a unique DNA-alkylating payload to achieve potent antitumor effects with good tolerability. The payload, DGN462, is prototypical of a novel class of purpose-created indolinobenzodiazeprine pseudodimers, termed IGNs. With low picomolar potency, IMGN779 reduced viability in a panel of AML cell lines *in vitro*. Mechanistically, the cytotoxic activity of IMGN779 involved DNA damage, cell-cycle arrest, and apoptosis consistent with the mode of action of DGN462. Moreover, IMGN779 was highly active against patient-derived AML cells, including those with adverse molecular abnormalities, and sensitivity correlated to CD33 expression levels. *In vivo*, IMGN779 displayed robust antitumor efficacy in multiple AML xenograft and disseminated disease models, as evidenced by durable tumor regressions and prolonged survival. Taken together, these findings identify IMGN779 as a promising new candidate for evaluation as a novel therapeutic in AML. *Mol Cancer Ther; 17(6); 1271–9. ©2018 AACR.*

Introduction

Acute myeloid leukemia (AML), an aggressive hematologic malignancy arising from bone marrow myeloid progenitor cells, remains the leading cause of mortality from leukemia in the United States (1). Standard induction treatment, based on cytarabine–anthracycline combination chemotherapy, can lead to complete remissions in up to 80% to 90% of cases, depending on patient age and mutational status of the underlying disease (2). However, even with these favorable primary response rates, relapse is unavoidable for a majority of individuals and 5-year overall survival rates remain disappointingly poor at 26% (3). Moreover, a disproportionate number of newly diagnosed cases occur in elderly patients who are less fit for intensive chemotherapy (4), and the outcomes of lower intensity treatments in this population are particularly dismal, with median overall survival often less than one year (5). An increased understanding of AML pathogenesis has identified a number of molecular candidates that serve as actionable targets for tailored therapeutic interventions in this disease, including a number of recurrent somatic mutations (e.g., *FLT3-ITD*) shown to directly impact disease progression, prognosis, and patient survival (6). Immunotherapeutic targeting strategies, designed to exploit defined antigens expressed on the surface of leukemic cells, represent another avenue that has been extensively investigated in the pursuit of novel treatments for AML patients (7). Such antibody-based approaches have been transformative for the management of other hematologic malignancies, most notably B-cell lymphomas (8); however, their full clinical potential is yet to be realized within the context of AML.

For close to three decades, a primary focus of antibody-directed therapy in AML has been CD33, a member of the sialic acid–binding receptor family and myeloid differentiation antigen that is broadly expressed on leukemic blasts in most patients (9). Although early attempts at targeting CD33 with unconjugated antibodies were disappointing (10), the endocytic properties of this receptor made it well suited for antibody–drug conjugate

[1]ImmunoGen, Inc., Waltham, Massachusetts. [2]Department of Hematology, VU University Medical Center, Amsterdam, the Netherlands. [3]Department of Medicine, Roswell Park Cancer Institute, Buffalo, New York.

Note: Supplementary data for this article are available at Molecular Cancer Therapeutics Online (http://mct.aacrjournals.org/).

Y. Kovtun and P. Noordhuis contributed equally to this article.

Corresponding Author: Yelena Kovtun, ImmunoGen, Inc., 830 Winter Street, Waltham, MA 02451. Phone: 781-895-0600; Fax: 781-895-0615; E-mail: Yelena.kovtun@immunogen.com

doi: 10.1158/1535-7163.MCT-17-1077

Published OnlineFirst March 27, 2018; DOI: 10.1158/1535-7163.MCT-17-1077

(ADC)-based strategies. ADCs are complex engineered molecules consisting of an mAb, directed toward tumor-associated antigens, conjugated via stable linkage to a potent cytotoxic agent (11). Clinical validation of this approach was provided by gemtuzumab ozogamicin (GO), an ADC comprised of an anti-CD33 antibody coupled to the potent DNA-targeting antitumor antibiotic calicheamicin (12), which received accelerated marketing approval for the treatment of AML in 2000 and was recently granted a second approval by the FDA in newly diagnosed and relapsed or refractory AML. However, safety concerns and limited potency of GO in multidrug resistant AML (10, 13) prompted the search for more effective ADCs, with superior therapeutic indices and favorable tolerability, to overcome such limitations. Accordingly, CD33 as a therapeutic target, as well as the ADC-based treatment modality, continue to be actively pursued within the setting of AML.

Currently, most clinical-stage ADCs utilize tubulin-directed small molecules as the payload, typically derivatives of the antimitotic microtubule-disrupting agents dolastatin 10 (i.e., auristatins; ref. 14), or maytansine (15). The early human trials of AVE9633, an ADC that targets CD33 for tumor-selective delivery of the maytansinoid compound DM4, revealed favorable tolerability but only modest activity in AML patients (16). Cytotoxic agents that target DNA are widely used in cancer therapy and, as exemplified by GO, there exists considerable interest in exploiting such mechanisms to produce more effective ADC therapies. In this regard, we have recently developed a new class of purpose-designed, highly cytotoxic compounds for use as effector molecules in ADCs known as IGNs, which consist of indolinobenzodiazeprine pseudodimers (17). It was determined that IGNs containing a diimine moiety act via both DNA-crosslinking and alkylation and, although highly active, exhibited unacceptable toxicity in mice. Modification to monoimine-containing forms of IGN changed the mechanism of action to DNA alkylation only, an effect that maintained potency while significantly improving tolerability. Optimized linker design resulted in identification of the lead molecule DGN462. ADCs generated using this DNA-alkylating payload are characterized by favorable safety and high therapeutic indices *in vivo* (17).

Here, we report on the preclinical characterization of a novel CD33-targeting and IGN-containing ADC, IMGN779, comprised of a humanized anti-CD33 antibody conjugated to DGN462 via a cleavable disulfide linker. IMGN779 demonstrates potent antitumor activity against AML cell lines and primary patient samples *in vitro*, as well as robust efficacy in multiple *in vivo* models of AML. These findings are of considerable translational relevance for further development of this unique class of DNA-alkylating ADCs and support the clinical advancement of IMGN779 as a potential treatment for AML with therapeutic advantages over existing agents.

Materials and Methods

Antibodies and reagents

The humanized anti-CD33 antibody Z4681A and a chimeric nontargeting control antibody, of the same IgG1 isotype and identical Fc sequences, were generated at ImmunoGen. IMGN779 and the control Ab-DGN462 ADC were produced via conjugation of DGN462 to the Z4681A and nontargeting IgG1 antibodies, respectively, using the cross-linking agent sulfo-SPDB [*N*-succinimidyl 2-sulfo-4-(2-pyridyldithio)butanoate] as described previously (17).

Cell lines and primary AML samples

The HEL92.1.7, HL60, HNT-34, Kasumi-1, KG-1, MV4-11, TF1, and TF1α human leukemia cell lines were purchased from ATCC. All other lines were obtained from DSMZ within the period of 2000 to 2015, characterized by the vendor using routine DNA profiling, and no further authentication was conducted by the authors. Cells were expanded and maintained as recommended by the vendors. Cell surface CD33 expression levels were determined using the QuantiBRITE fluorescence quantification system (BD Biosciences) according to the manufacturer's protocol. Briefly, cells were incubated on ice for one hour with 1.5 μg/mL of CD33-PE conjugate plus 10% human serum (Sigma-Aldrich; to block Fc receptors). Cells were then washed, fixed, and analyzed by flow cytometry. To determine antibody bound per cell (ABC) values, QuantiBRITE PE beads (BD Biosciences) were run using identical instrument settings as the cells, and the data were used to generate a standard curve with FlowJo software. P-glycoprotein efflux activity was assessed using a flow cytometric method, in which cells were incubated with 0.3 pg/mL of the green fluorescent nucleic acid stain SYTO16 in either the absence or presence of the 2.4 μg/mL P-glycoprotein inhibitor PSC833 (18).

Primary AML samples were obtained from the HOVON/SAKK 102 and 103 clinical studies, which were reviewed and approved by an Institutional Review Board of the Erasmus MC (Rotterdam, the Netherlands), and conducted in accordance with the Declaration of Helsinki. All patients provided their written informed consent to participate in the trials. Details of the clinical studies can be found at www.hovon.nl. Samples were characterized by multiparametric flow cytometry. AML leukemic progenitors (LP) were defined as SSCmed/$CD34^+$/$CD38^+$ population. The CD33 ABC values and P-glycoprotein efflux activity on the progenitors were assessed as described above for the cell lines.

Binding and internalization assays

To measure binding affinity, $CD33^+$ HNT-34 cells were incubated for 2 hours at 4°C with serial dilutions of Z4681A and IMGN779, followed by addition of the FITC-conjugated goat anti-human IgG-antibody (The Jackson Laboratory) for an additional 60 minutes. Cells were analyzed using a FACSCalibur flow cytometer (BD Biosciences) and data analysis was performed using CellQuest Pro software (BD Biosciences).

To assess antibody internalization, HNT-34 or EOL-1 cells were incubated with 10 nmol/L of Alexa Fluor 488–labeled Z4681A or nonbinding human IgG1 control (Ab-AF488) at 37°C. At selected time points up to 24 hours, cell surface–associated fluorescence was quenched with 20 μg/mL of anti-Alexa Fluor 488 antibody (Invitrogen), and internalized fluorescence signals were quantified by flow cytometry and analyzed with FlowJo software (FlowJo LLC).

Radiolabeled processing studies

Tritium-labeled IMGN779 (^{3}H-IMGN779; Z4681A-sulfo-SPDB-[^{3}H]DGN462) was prepared by first modifying the Z4681A antibody with the sulfo-SPDB linker to incorporate thiopyridine groups. The modified antibody (2 mg/mL) in pH 8.5-buffered aqueous solution (15 mmol/L HEPES) containing 15% DMA was treated with sulfonated [^{3}H]DGN462 (1.3 equivalents per thiopyridine group). The reaction mixture was incubated overnight, followed by purification and formulation into the final buffer (20 mmol/L histidine, 8% trehalose, 50 μmol/L sodium bisulfite, pH 6.1). The nontargeting control conjugate (Ab-

Published OnlineFirst March 27, 2018; DOI: 10.1158/1535-7163.MCT-17-1077

[^{3}H]DGN462) was prepared in a similar manner. EOL-1 cells were exposed to a 30-minute pulse with 3 nmol/L ^{3}H-IMGN779 or Ab-[^{3}H]DGN462. Cells were washed and cultured for 22 hours at 37°C, harvested, and extracted with organic solvent to separate soluble ^{3}H-containing species from protein-associated species. Radioactivity was measured by liquid scintillation counting using a Tri-Carb 2900T counter (Packard BioScience) and calculated on the basis of counts per minute (CPM) values. The picomoles of ^{3}H-labeled catabolite per million cells were determined using the following equation: (CPM extract/million cells) × (1 dpm/0.6 CPM) × (1 mCi/2.2 × 10^9 dpm) × [1/conjugate-specific radioactivity (mCi/mmol)] × 10^9. Values were then normalized to picomoles of degraded antibody/million cells by dividing the results by the molar ratio of [^{3}H]-label for ^{3}H-IMGN779 or Ab-[^{3}H]DGN462.

Cell cycle, DNA damage, and apoptosis assays

For cell-cycle analysis, MV4-11 cells were incubated with 1 nmol/L of IMGN779 for 48 hours at 37°C prior to harvest. Cells were fixed, washed, and stained with propidium iodide before total DNA content was analyzed by flow cytometry and analyzed using ModFit software (Verify Software House). For the DNA damage and apoptosis assays, MV4-11 cells were treated with 1 nmol/L IMGN779 and harvested at time intervals between 2 and 48 hours. Cells were stained with phosphorylated H2AX (pS139; BD Biosciences) and cleaved caspase-3 (Asp175; Cell Signaling Technology) antibodies, prior to flow cytometry and analysis using FlowJo software.

In vitro cytotoxicity

For the panel of AML lines, cytotoxicity was assessed using a water-soluble tetrazolium salt-8 (WST-8)–based cell viability assay (Dojindo Molecular Technologies) as described previously (19). Briefly, exponentially growing AML cells were seeded into 96-well plates and incubated in the presence of increasing concentrations of IMGN779 or DGN462, for 4 days at 37°C. Cell viability was determined from background corrected WST-8 absorbance, with all assays performed in triplicate. The surviving fractions were calculated by dividing the viability value for each treatment by the viability value in the control (untreated) wells and plotting against the test article concentrations to estimate IC_{50} values.

For the studies with primary patient samples, cytotoxicity was assessed using a colony-forming units assay. LP and normal bone marrow mononuclear cells were treated with serial dilutions of IMGN779 at 37°C in a humidified 5% CO_2 incubator for 20 hours. Treated cells were then mixed with MethoCult (Stem Cell Technologies) supplemented with IL3, SCF, and Flt-3 (all 50 ng/mL; Humanzyme) and seeded into 6-well plates. Plates were incubated for 7 to 14 days until colonies formed. Colonies were counted under a microscope and IC_{50} values were estimated by dividing the number of colonies for each treatment by the control number of colonies, plotted against IMGN779 concentrations.

In vivo xenograft tumor models

Female athymic nude, CB.17 SCID, and NOD/SCID mice were obtained from Charles River Laboratories and IL2 receptor gamma chain–deficient NOD/SCID mice (NSG) from The Jackson Laboratory. All animal procedures were performed in strict accordance with ImmunoGens' Animal Care and Use Committee, Roswell Park Cancer Institute's Animal Care and Use Committee, and the NIH Guide for the Care and Use of Laboratory Animals. Nude and CB.17 SCID mice were inoculated subcutaneously with EOL-1 or MV4-11 tumor cells (10^7 cells/mouse), respectively, and animals were randomized into treatment groups (6 mice/group) when the mean tumor volume of the cohorts reached approximately 120 to 125 mm^3. Mice received 400 mg/kg human IgG1 intraperitoneally 24 hours prior to initiation of therapy to block Fc receptor (FcR)-mediated uptake of test articles, and additional doses at 100 mg/kg on days 5 and 10 postdosing to maintain adequate plasma concentrations. EOL-1 tumor-bearing mice received a single intravenous bolus administration of vehicle, IMGN779, or Ab-DGN462, with each conjugate molecule dosed at approximately 0.5 or 1.5 mg/kg ADC by antibody concentration (i.e., 10 or 30 μg/kg linked IGN). IMGN779 was administered to mice bearing MV4-11 xenografts as a single dose of 0.5 mg/kg on day 1, or as two doses of 0.25 mg/kg on either days 1 and 4 or days 1 and 8. For both models, tumor volumes (TV) were recorded 2 to 3 times weekly by caliper measurements of the height (H), length (L), and width (W) of the tumor, following the formula TV = $(H \times L \times W)/2$. Tumor growth inhibition (T/C value) was expressed as a percentage of growth inhibition of tumors in the treatment group (T) compared with the control (vehicle) group (C), when the control group's mean TV reached approximately 800 mm^3.

To model systemic disease, NOD/SCID mice (pretreated with 150 mg/kg cyclophosphamide on days 2 and 3 prior to cell inoculation) were injected intravenously via the tail vein with 3 × 10^6 MV4-11 cells suspended in serum-free culture medium. Animals were dosed intraperitoneally with 400 mg/kg human IgG1 to block FcR on day 6 postinoculation and randomly divided into 3 groups ($n = 10$ mice/group) based on body weight. On day 7, mice were administered a single intravenous dose of vehicle (PBS), 0.5 mg/kg IMGN779, or 0.5 mg/kg Ab-DGN462. Survival was followed for up to 150 days. For the systemic study using luciferase-labeled tumor cells, NSG mice were sublethally irradiated (200 rad) and allowed to rest for 2 hours, followed by tail vein injection of 1 × 10^7 MV4-11 cells stably transfected with a pGL4 luciferase reporter vector (Promega). Mice were evaluated weekly for evidence of leukemia engraftment and overall disease progression by serial dorsal and ventral bioluminescent imaging (BLI; Xenogen IVIS Spectrum System, Caliper Life Sciences) after intraperitoneal D-luciferin (Gold Bio) injection (15 mg/kg). The average photon emission in photons per second per cm^2 per steradian was calculated from averaging dorsal and ventral images from each animal at each time point (Living Imaging Software, PerkinElmer). Seven days postinoculation, engrafted animals ($n = 5$ mice/group) were intraperitoneally administered 400 mg/kg blocking antibody. Twenty-four hours later, animals were treated with a single intravenous dose of vehicle (20 mmol/L histidine, 8% trehalose, 50 μmol/L bisulfite, and 0.02% polysorbate) or 1.5 mg/kg IMGN779. In both disseminated models, mice were continuously monitored and removed from study when advanced health distress signs were observed (hind leg paralysis, tumor growth on body, or moribund state) or measured (>20% loss of initial body weight).

Results

Validation of IMGN779 design and mechanism of action

IMGN779 was generated through conjugation of DGN462, a member of our novel class of DNA-interacting IGN molecules

Published OnlineFirst March 27, 2018; DOI: 10.1158/1535-7163.MCT-17-1077

(17), to the humanized anti-CD33 antibody Z4681A (Fig. 1A). ADC optimization led to the use of a cleavable disulfide linker (sulfo-SPDB), which, along with further reversible sulfonation of the imine moiety of DGN462, conferred improved solubility and tolerability to the resulting conjugate (17). The relative binding affinities of Z4681A and IMGN779, evaluated by flow cytometry in the $CD33^+$ AML cell line HNT-34, are shown in Fig. 1B. Both the unconjugated antibody and intact ADC bound with similar high affinity, suggesting that incorporation of DGN462 (approximately 3 molecules/antibody) via the sulfo-SPDB linker in IMGN779 did not exert a major impact on antigen-specific binding.

The biological activity of an ADC is reliant on internalization and intracellular processing of the conjugate molecule to release the cytotoxic payload. Internalization of Z4681A, the antibody component of IMGN779, is presented for two $CD33^+$ AML lines in Fig. 1C. HNT-34 and EOL-1 cells were incubated with fluorescently labeled Z4681A (Z4681A-AF488) or nontargeting antibody (Ab-AF488) for up to 24 hours. Fluorescence of each internalized ADC was measured by flow cytometry after quenching of the surface-bound AF488 with an anti-AF488 antibody. In each cell line, rapid internalization and intracellular accumulation of Z4681A, but not the control antibody, was observed. Next, *in vitro* processing was evaluated in EOL-1 cells, using tritium-labeled IMGN779 (^{3}H-IMGN779) and a nontargeting control conjugate (Ab-[^{3}H]DGN462). The amount of total catabolite produced following a 30-minute pulse exposure to 3 nmol/L of either reagent was calculated, taking into account both the quantity of antibody bound and the percent degraded (Fig. 1D). The amount of catabolite generated from Ab-[^{3}H]DGN462 was negligible (0.0004 pmol catabolite per million cells); however, the concentration observed following treatment with ^{3}H-IMGN779 was 10-fold higher. This result is consistent with enhanced processing and generation of higher concentrations of cytotoxic catabolite species as a consequence of selective, target-mediated uptake and degradation of IMGN779 in $CD33^+$ AML cells.

IMGN779 induces DNA damage, cell-cycle arrest, and apoptosis

A series of experiments were undertaken in the $CD33^+$ MV4-11 AML cell line, which contains an activating FLT3-ITD mutation, to examine the cellular consequences of IMGN779 treatment. Cell-cycle analysis revealed that IMGN779 exposure resulted in the S-phase accumulation, G_2–M arrest, and the appearance of a sub-

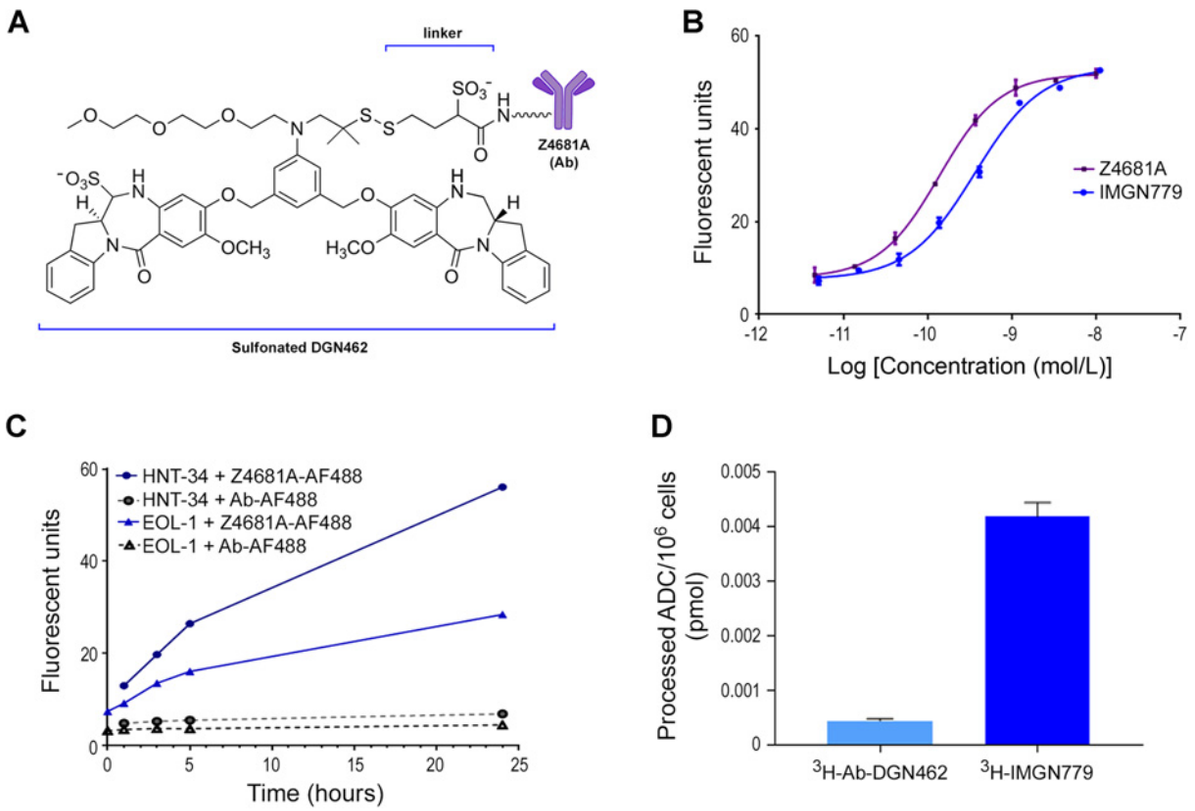

Figure 1.

Structure, binding, and internalization of the CD33-targeting ADC, IMGN779, and its antibody moiety Z4681A. **A,** Chemical structure of IMGN779. **B,** Relative binding affinities of Z4681A and IMGN779 on HNT-34 AML cells. HNT-34 cells were cultured with the indicated concentrations of either the unconjugated antibody or intact ADC, and binding was detected by flow cytometry using a fluorescently labeled anti-human antibody. **C,** HNT-34 or EOL-1 cells were incubated with 10 nm of AF488-labeled Z4681A, or nonbinding control antibody, for 24 hours at 37°C. At the indicated time points, cell surface–associated fluorescence was quenched with anti-AF488 antibody, and internalized fluorescent signals were quantified by flow cytometry. **D,** EOL-1 cells were pulse-treated with 3 nmol/L ^{3}H-Ab-DGN462 or ^{3}H-IMGN779 for 30 minutes and then cultured for 22 hours at 37°C. The amount of catabolite (processed ADC) was calculated from the processed CPM values from protein-free extracts, converted to picomoles of catabolite per million cells, and normalized for the drug–antibody ratio of each conjugate.

Published OnlineFirst March 27, 2018; DOI: 10.1158/1535-7163.MCT-17-1077

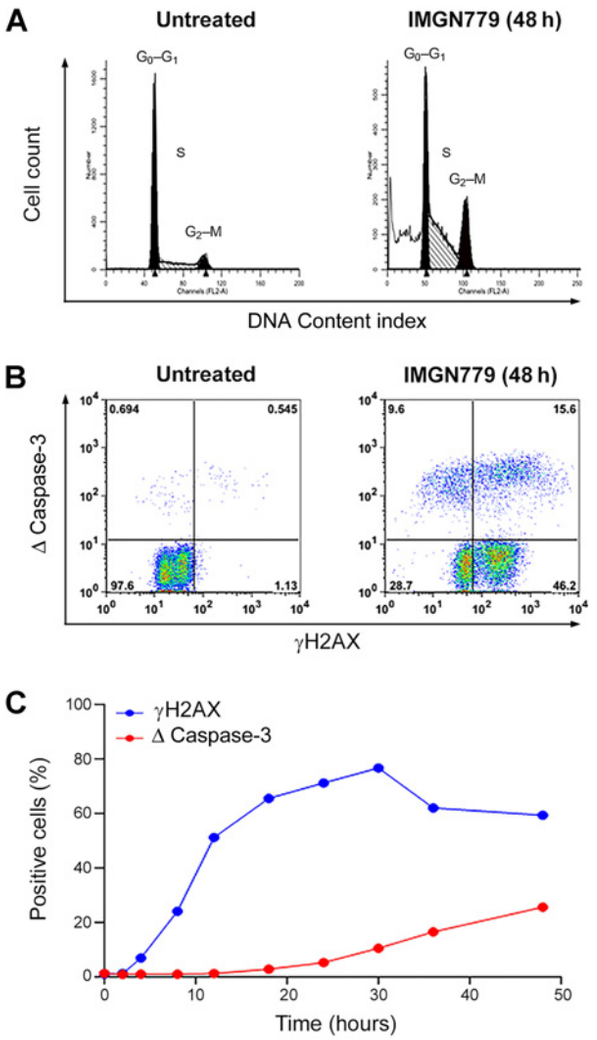

Figure 2.

IMGN779 effects on cell cycle, DNA damage, and apoptosis in MV4-11 AML cells. MV4-11 cells were continuously exposed to 1 nmol/L IMGN779 and compared with control (untreated) cells. **A,** Cell-cycle distribution was determined by flow cytometry 48 hours posttreatment. **B,** γ-H2AX and cleaved caspase-3 (Δ caspase-3) expression determined at 48 hours. **C,** Kinetic analysis of γ-H2AX and cleaved caspase-3 induction in MV4-11 cells following exposure to IMGN779.

G_0–G_1 population by 48 hours (Fig. 2A). At this same time point, corresponding elevations in the apoptotic marker cleaved caspase-3 as well as phosphorylated histone H2AX (γ-H2AX) levels were observed (Fig. 2B). γ-H2AX is an early and sensitive indicator of DNA damage that is induced in response to alkylating agents (20). Closer examination of the kinetics of its induction showed a rapid increase in expression that was evident within 4 to 8 hours and peaked at 30 hours post-treatment (Fig 2C). Importantly, this temporal response preceded that of caspase activation. Taken together, these data indicate that the cytotoxic activity of IMGN779 arises, at least in part, as a consequence of payload-induced DNA damage, leading to cell-cycle arrest and apoptosis.

IMGN779 displays potent cytotoxic activity in AML cell lines

The *in vitro* cytotoxic activity of IMGN779 was determined against a panel of leukemic cell lines that exhibited a range of CD33 expression levels (Table 1). IMGN779 was potently cytotoxic in the majority of lines examined, typically with IC_{50} values in the picomolar range. No significant correlation between IMGN779 activity and CD33 expression was observed (Supplementary Fig. S1A); however, the strong relationship between sensitivity to IMGN779 and to DGN462 alone (Supplementary Fig. S1B) suggests that the ADC activity in this collection of established AML lines was payload- rather than antigen-driven. Of note, IMGN779 showed considerably greater potency than the maytansinoid-containing AVE9633 (up to 3 logs), when the two CD33-targeting ADCs were directly compared (Supplementary Table S1).

Ex vivo cytotoxicity of IMGN779 against $CD33^+$ primary AML progenitor cells

To extend these observations, the activity of IMGN779 against LPs was evaluated in diagnostic specimens from 50 patients with AML (Table 2). IMGN779 demonstrated picomolar potency against the majority of primary progenitors examined, which harbored a range of mutational phenotypes characteristic of AML (Table 2). Target antigen levels and drug transporter expression are key influencers of ADC activity (21). In this regard, P-glycoprotein activity, a primary contributor to multidrug resistance, varied widely in this collection of patient samples, and only a weak relationship between this parameter and IMGN779 potency was seen (Supplementary Fig. S2). However, additional relationship analyses revealed that LP expression levels of CD33 strongly correlated with IMGN779 sensitivity [Spearman correlation coefficient (r) = −0.4755, P = 0.001; Fig. 3]. Importantly, IMGN779 showed reduced activity against normal bone marrow cell samples taken from healthy donors (Supplementary Table S2).

In vivo antitumor efficacy of IMGN779 in AML models

To determine whether the potent *in vitro* effects of IMGN779 translated to *in vivo* antitumor activity, we examined the efficacy of IMGN779 treatment in a series of AML xenograft models. We had previously established that IMGN779 was well tolerated at doses up to approximately 48 mg/kg (i.e., 950 μg/kg linked IGN;

Table 1. IMGN779 *in vitro* cytotoxicity in leukemic cell lines

Cell line	IMGN779 IC_{50} (pmol/L)	CD33 ABC
CMK	700	54,589
CMK-86	39	19,605
EOL-1	14	9,692
HEL	500	35,224
HEL92.1.7	40	39,353
HL60s	28	24,943
KG-1	≥1,000	6,801
ML-2	17	15,995
MOLM-13	8	44,354
MV4-11	5	17,757
NB4	400	10,493
OCI-AML2	30	13,760
OCI-AML4	10	13,534
OCI-M1	10	55,353
OCI-M2	≥1,000	3,345
PL-21	≥1,000	21,153
SKM-1	7	14,033
TF1	230	65,088
TF1-α	≥1,000	34,703

Published OnlineFirst March 27, 2018; DOI: 10.1158/1535-7163.MCT-17-1077

Table 2. *In vitro* cytotoxicity of IMGN779 against primary AML progenitor cells

Sample #	IC_{50} (pmol/L)	CD33 expression (LP)	Mutations	P-glycoprotein activity
43	10	10,881	FLT3-ITD, NPM1	2.1
50	11	8,572	FLT3-ITD	2.5
10	16	6,893	Negative	1.0
8	22	12,567	ND	1.1
47	26	1,084	Negative	1.6
17	27	11,191	FLT3-ITD	1.1
56	28	8,101	NPM1	1.9
5	29	8,508	FLT3-ITD	0.3
53	35	7,676	FLT3-ITD, NPM1	1.6
46	38	15,988	FLT3-ITD	1.8
65	48	10,211	CEPBα	2.0
29	63	6,922	FLT3-ITD, NPM1	1.5
11	87	15,574	FLT3-ITD, NPM1	0.8
33	89	1,739	NPM1	1.9
27	91	8,442	FLT3-ITD, NPM1	1.2
45	107	3,312	c-KIT	1.1
58	110	8,759	NPM1	1.6
15	112	2,193	ND	1.2
24	124	11,269	Negative	1.2
39	139	954	FLT3-ITD, NPM1, CEPBα	2.8
52	139	13,956	FLT3-ITD, NPM1	1.1
63	144	11,961	negative	2.3
61[a]	158	11,141	FLT3-ITD, NPM1	1.5
48	195	3,356	FLT3-ITD	1.6
35	206	6,932	FLT3-ITD, NPM1	1.2
55	207	11,701	FLT3-ITD, NPM1	1.3
19	214	983	Negative	1.3
13	218	1,251	FLT3-ITD	1.3
57	227	7,809	FLT3-ITD	1.3
42	268	3,599	FLT3-ITD	2.3
36	285	3,136	FLT3-ITD	1.8
32	290	4,831	Negative	2.6
28	302	4,633	FLT3-ITD, NPM1	1.6
38	381	2,034	Negative	2.4
6	404	1,237	ND	1.2
16	480	3,893	ND	2.2
64	581	3,184	NPM1	1.8
1	583	554	Negative	1.9
68	647	4,812	CEPBα	5.0
20	735	3,767	FLT3-ITD, NPM1	1.0
37	912	2,405	JAK2	2.2
7	929	1,330	ND	1.8
34	1,196	903	Negative	2.2
12	1,234	1,040	Negative	1.6
21	1,357	2,183	Negative	1.6
40	1,453	213	Negative	2.3
22	1,479	3,384	ND	2.2
54	1,668	3,796	FLT3-ITD	1.9
60[a]	2,006	7,599	FLT3-ITD, NPM1	1.4
62[a]	2,095	5,597	Negative	3.1

[a]Samples 60, 61, and 62 are from relapsed (60) and refractory patients (61, 62). All others were obtained at the time of diagnosis.

Supplementary Fig. S3A); the starting dose for the efficacy studies was approximately 100-fold lower. In the initial set of experiments, EOL-1 tumor-bearing mice received a single administration of IMGN779, or the nontargeting ADC (Ab-DGN462) as a control, at either 0.5 or 1.5 mg/kg (Fig. 4A). Treatment with 0.5 mg/kg Ab-DGN462 had no effect on tumor growth, whereas the higher dose induced only a moderate and transient growth delay. In stark contrast, IMGN779 monotherapy was highly active. Tumor growth was inhibited by 97% (i.e., T/C value of 3% on day 15) in the 0.5 mg/kg–treated group, and completely abrogated by 1.5 mg/kg dosing, which induced complete and sustained regressions (out to 90 days) in 6 of 6 animals. All regimens were well tolerated, with no body weight loss seen over the course of the study (Supplementary Fig. S3B).

Next, the effects of fractionated dosing were examined whereby mice bearing MV4-11 xenografts were administered IMGN779 as a single 0.5 mg/kg dose or two 0.25 mg/kg doses, administered either 3 days or one week apart (Fig. 4B). Both split-dosing regimens showed an identical degree of growth inhibition on day 31 (T/C values of 0%) as the single 0.5 mg/kg administration. However, each fractionated dose group had 33% more tumor-free surviving animals at the end of study compared with the single dose group (5/6 vs. 3/6, respectively). All schedules were well tolerated (Supplementary Fig. S3C).

The MV4-11 line was also used to evaluate the overall survival benefit of IMGN779 treatment in two disseminated leukemia models. In the first study, NOD/SCID mice were inoculated with MV4-11 cells and induction of therapy delayed until day 7 to

Published OnlineFirst March 27, 2018; DOI: 10.1158/1535-7163.MCT-17-1077

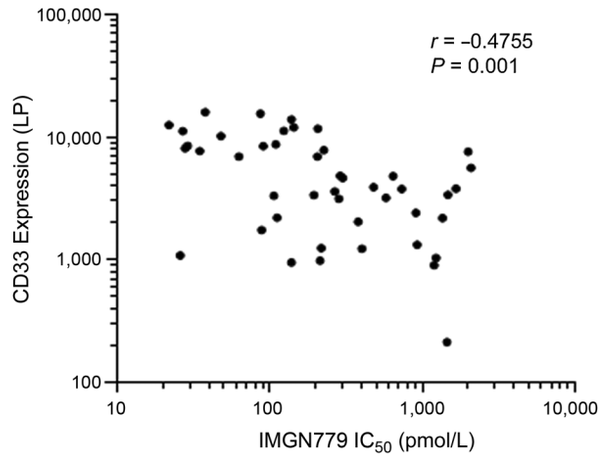

Figure 3.
Relationship between IMGN779 sensitivity and CD33 expression on patient-derived LP cells. The correlation between the rank of IMGN779 IC_{50} values and CD33 levels (ABC values) is visualized. The Spearman correlation coefficient (r) was −0.4755 ($P = 0.001$).

allow engraftment and outgrowth of AML cells. Animals were dosed with a single administration of IMGN779 or Ab-DGN462 (each at 0.5 mg/kg). As shown in the Kaplan–Meier curves (Fig. 4C), all vehicle-treated animals succumbed to disease by day 60 postinoculation, and Ab-DGN462 treatment had no effect on median or overall survival. IMGN779 therapy was highly active however, as evidenced by a >90% increased life span and one animal still alive at the end of the study (day 150).

In the second study, NSG mice were systemically engrafted with luciferase-transfected MV4-11 cells and dosed with either vehicle or 1.5 mg/kg IMGN779. Induction of therapy was again delayed for 7 days following inoculation; survival and disease burden were subsequently monitored out to day 81 posttreatment (Fig. 4D). Representative whole-animal BLI on day 28 posttreatment is shown in Fig. 4E. All animals in the control group had widespread disease burden and were off-study between days 32 and 34 due to disease progression. In agreement with the highly efficacious activity observed in the EOL-1 xenograft model (Fig. 4A), this dose of IMGN779 completely inhibited AML growth, with all mice surviving the duration of the study and no evidence of leukemic disease discernible by luminescence at either day 28 (Fig. 4E) or at the end of the experiment (day 81).

Discussion

IMGN779 is a CD33-targeting ADC that utilizes DGN462 as its payload, prototypical of the recently developed IGN class of highly potent DNA alkylators (17). IGNs were designed to provide DNA-interacting effector molecules that satisfied key criteria for incorporation into ADCs. These included high potency,

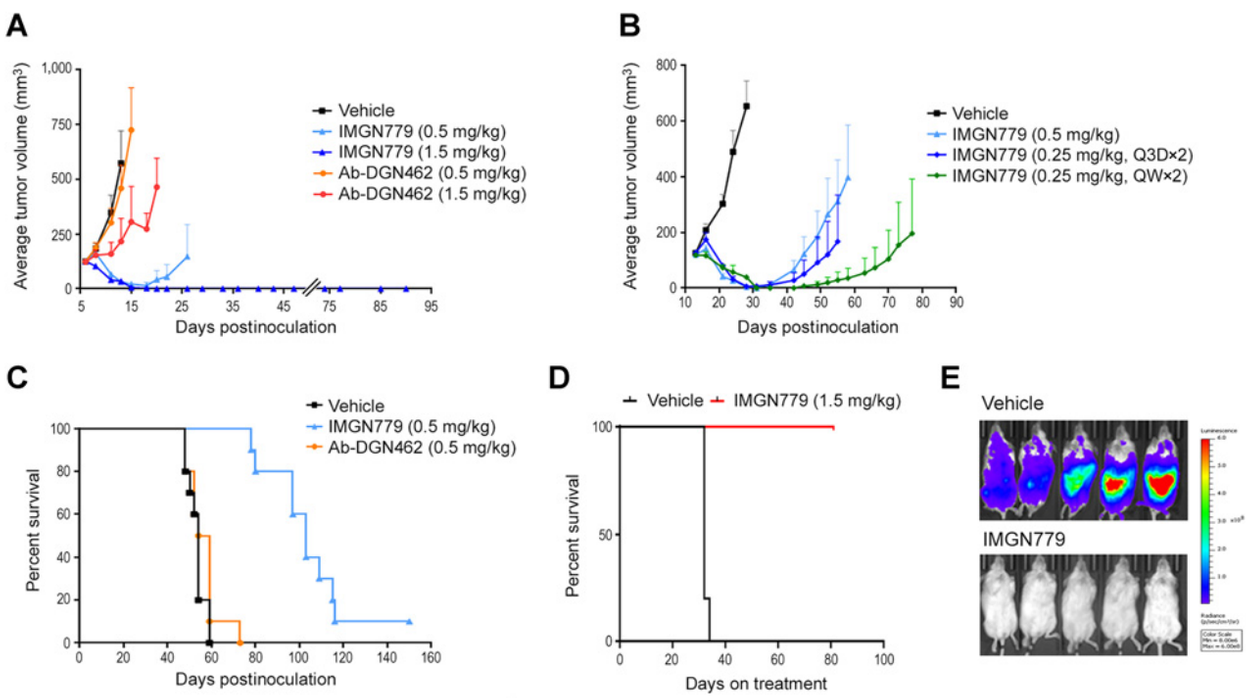

Figure 4.
IMGN779 exhibits potent *in vivo* antitumor efficacy in models of AML. **A,** Nude mice bearing EOL-1 xenografts were dosed with vehicle, a single dose of IMGN779 (0.5 or 1.5 mg/kg), or a single dose of Ab-DGN462 (0.5 or 1.5 mg/kg), as indicated. **B,** SCID mice bearing MV4-11 xenografts were treated with vehicle, a single dose of 0.5 mg/kg IMGN779, two doses of 0.25 mg/kg IMGN779 3 days apart (Q3D×2), or two doses of 0.25 mg/kg IMGN779 1 week apart (QW×2), as indicated. **C,** Kaplan–Meier analysis of overall survival in a disseminated MV4-11 model. Beginning 7 days after tumor cell inoculation, NOD/SCID mice were administered a single dose of vehicle, 0.5 mg/kg IMGN779, or 0.5 mg/kg Ab-DGN462, and animal survival monitored out to 150 days. **D,** Kaplan–Meier analysis of overall survival. Seven days after MV4-11-luciferase tumor cell inoculation, NOD/SCID mice were administered a single dose of vehicle or 1.5 mg/kg IMGN779, and animal survival was monitored for 81 days posttreatment. **E,** Representative BLI per animal per treatment group on day 28.

Published OnlineFirst March 27, 2018; DOI: 10.1158/1535-7163.MCT-17-1077

stability, and solubility in aqueous formulation, as well as conferring effective therapeutic indices as ADCs *in vivo* (17). Consistent with the monofunctional alkylating activity of DGN462, exposure of $CD33^+$ AML cells to IMGN779 resulted in rapid induction of γ-H2AX, a sensitive marker of DNA damage, which was subsequently followed by cell-cycle arrest and apoptosis. IMGN779 was potently cytotoxic (with IC_{50} values in the picomolar range) against AML lines *in vitro* and was remarkably more active than AVE9633, a first-generation ADC utilizing an antibody "backbone" that recognizes the same CD33 epitope as Z4681A but conjugated to the maytansinoid DM4. It is well established that the multidrug resistant phenotype is a negative prognostic factor with respect to chemotherapeutic response in AML (22, 23). More specifically, P-glycoprotein activity has been shown to be an important factor in attenuating both AVE9633 and DM4 cytotoxicity in leukemic cell lines (24) and is also a key mechanism associated with resistance to GO (25–27). The finding that IMGN779 was potently cytotoxic to patient-derived progenitors that harbored a range of adverse cytogenetic and molecular abnormalities, including those with active P-glycoprotein transporter, is of direct translational relevance for the potentially broad therapeutic applicability of this ADC in AML.

IMGN779 was designed to overcome the limitations of earlier CD33-targeting ADCs, such as GO (9) and AVE9633. Like in GO, a DNA-interacting payload was used in the development of vadastuximab talirine (SGN-CD33A), which comprises a humanized CD33 antibody engineered for site-specific conjugation of a synthetic pyrrolobenzodiazepine (PBD) dimer via a protease-cleavable linker (28). PBDs are a class of cytotoxic, DNA minor-groove binding agents, originally isolated from a strain of *Streptomyces* (29). The early clinical evaluations of vadastuximab talirine in AML, both as monotherapy and in combination with the hypomethylating agents (HMA) azacitidine or decitabine, revealed encouraging signals of efficacy (30, 31). Adverse events were primarily related to myelosuppression, which is not unexpected with an effective CD33-targeted agent, given the expression of this antigen on normal hematopoietic cells. These results led to initiation of the pivotal phase III CASCADE trial evaluating HMA with or without vadastuximab talirine in older patients with newly diagnosed AML (NCT02785900). Unfortunately, the CASCADE trial was recently discontinued owing to a higher rate of deaths, including fatal infections, in the vadastuximab talirine–containing arm versus the HMA control arm of the study. These safety issues appear distinct from an elevated risk of hepatotoxicity, including transplant-associated hepatic veno-occlusive disease/sinusoidal obstruction syndrome, which was first identified with GO therapy but also emerged as a concern for this particular ADC (32).

A key observation of the current study was the potent *in vivo* antitumor activity and good tolerability exhibited by IMGN779 when administered as a single 0.5 mg/kg dose in both subcutaneous xenograft and disseminated AML models. Treatment at a 3-fold higher level completely abrogated tumor growth and induced durable remissions in EOL-1 xenograft tumors and was curative for disseminated MV4-11 disease, a finding that was confirmed by imaging studies. Of note, these doses represent only approximately 1% to 3% of maximally tolerated levels for this conjugate molecule in mice, with the caveat that the Z4681A antibody component in IMGN779 is not cross-reactive with murine CD33. In all cases, the antitumor activity was target-specific, as a non-binding control ADC exhibited only marginal activity at the highest dose examined. Moreover, IMGN779 was found to be highly efficacious and well tolerated in repeat-dosing regimens, where additional benefit was achieved with fractionating the dosing regimen over a single, higher administration. Interestingly, the recent broad label reapproval of GO for adults with newly diagnosed $CD33^+$ AML, and in adult or pediatric patients with relapsed/refractory $CD33^+$ disease, was dependent on revised dosing paradigms, including intermittent administration schedules, which conferred improved tolerability without impacting clinical activity (33). Overall, the potent and durable response properties of IMGN779 may additionally support the use of intermittent dosing schedules in the clinical setting, a factor that would be further expected to contribute to a favorable activity profile.

Overall, we have developed and characterized a novel CD33-targeting ADC that employs a unique cytotoxic payload to achieve potent antitumor activity in preclinical models of AML. The findings presented here identify IMGN779 as a promising new therapeutic candidate for the treatment of this disease. In this regard, the clinical evaluation of IMGN779 has commenced, with a phase I study in patients with relapsed/refractory $CD33^+$ AML (NCT02674763) currently underway.

Disclosure of Potential Conflicts of Interest

E.S. Wang reports receiving a commercial research grant from and is a consultant/advisory board member for ImmunoGen, Inc. No potential conflicts of interest were disclosed by the other authors.

Authors' Contributions

Conception and design: Y. Kovtun, P. Noordhuis, K.R. Whiteman, G. Ossenkoppele, J. Pinkas

Development of methodology: Y. Kovtun, P. Noordhuis, K.R. Whiteman, L. Harvey, K.C. Lai, G.J. Schuurhuis

Acquisition of data (provided animals, acquired and managed patients, provided facilities, etc.): P. Noordhuis, K.R. Whiteman, K. Watkins, G.E. Jones, L. Harvey, K.C. Lai, G.J. Schuurhuis, E.S. Wang, J. Pinkas

Analysis and interpretation of data (e.g., statistical analysis, biostatistics, computational analysis): Y. Kovtun, P. Noordhuis, K.R. Whiteman, K. Watkins, G.E. Jones, L. Harvey, S. Adams, C.M. Sloss, G.J. Schuurhuis, G. Ossenkoppele, E.S. Wang

Writing, review, and/or revision of the manuscript: Y. Kovtun, P. Noordhuis, K.R. Whiteman, K.C. Lai, S. Adams, C.M. Sloss, G.J. Schuurhuis, G. Ossenkoppele, E.S. Wang, J. Pinkas

Administrative, technical, or material support (i.e., reporting or organizing data, constructing databases): L. Harvey, S. Portwood, S. Adams, G. Ossenkoppele

Study supervision: Y. Kovtun, S. Adams, C.M. Sloss, J. Pinkas

Acknowledgments

All work was funded by ImmunoGen, Inc. We wish to thank our colleagues Barbara Leece, Russell Walker, Katie O'Callaghan, and Holly Johnson-Modafferi for their contributions to the current study. We also want to sincerely thank Ravi Chari and Michael Miller for their invaluable contributions in design and development of IMGN779 and thoughtful review of this work. We also thank Dr. Richard Bates who provided drafts and editorial assistance during production of this manuscript.

The costs of publication of this article were defrayed in part by the payment of page charges. This article must therefore be hereby marked *advertisement* in accordance with 18 U.S.C. Section 1734 solely to indicate this fact.

Received November 6, 2017; revised January 18, 2018; accepted March 23, 2018; published first March 27, 2018.

References

1. Siegel RL, Miller KD, Jemal A. Cancer statistics, 2017. CA Cancer J Clin 2017;67:7–30.
2. Hackl H, Astanina K, Wieser R. Molecular and genetic alterations associated with therapy resistance and relapse of acute myeloid leukemia. J Hematol Oncol 2017;10:51.
3. Saygin C, Carraway HE. Emerging therapies for acute myeloid leukemia. J Hematol Oncol 2017;10:93.
4. Medeiros BC, Satram-Hoang S, Hurst D, Hoang KQ, Momin F, Reyes C. Big data analysis of treatment patterns and outcomes among elderly acute myeloid leukemia patients in the United States. Ann Hematol 2015;94: 1127–38.
5. Podoltsev NA, Stahl M, Zeidan AM, Gore SD. Selecting initial treatment of acute myeloid leukaemia in older adults. Blood Rev 2017;31:43–62.
6. Al-Issa K, Nazha A. Molecular landscape in acute myeloid leukemia: where do we stand in 2016. Cancer Biol Med 2016;13:474–82.
7. Garfin PM, Feldman EJ. Antibody-based treatment of acute myeloid leukemia. Curr Hematol Malig Rep 2016;11:545–52.
8. Ku M, Chong G, Hawkes EA. Tumour cell surface antigen targeted therapies in B-cell lymphomas: beyond rituximab. Blood Rev 2017;31:23–35.
9. Laszlo GS, Estey EH, Walter RB. The past and future of CD33 as therapeutic target in acute myeloid leukemia. Blood Rev 2014;28:143–53.
10. Jurcic JG. What happened to anti-CD33 therapy for acute myeloid leukemia? Curr Hematol Malig Rep 2012;7:65–73.
11. Chari RV, Miller ML, Widdison WC. Antibody-drug conjugates: an emerging concept in cancer therapy. Angew Chem Int Ed Engl 2014; 53:3796–827.
12. Cowan AJ, Laszlo GS, Estey EH, Walter RB. Antibody-based therapy of acute myeloid leukemia with gemtuzumab ozogamicin. Front Biosci (Landmark Ed) 2013;18:1311–34.
13. Petersdorf SH, Kopecky KJ, Slovak M, Willman C, Nevill T, Brandwein J, et al. A phase 3 study of gemtuzumab ozogamicin during induction and postconsolidation therapy in younger patients with acute myeloid leukemia. Blood 2013;121:4854–60.
14. Doronina SO, Toki BE, Torgov MY, Mendelsohn BA, Cerveny CG, Chace DF, et al. Development of potent monoclonal antibody auristatin conjugates for cancer therapy. Nat Biotechnol 2003;21:778–84.
15. Widdison WC, Wilhelm SD, Cavanagh EE, Whiteman KR, Leece BA, Kovtun Y, et al. Semisynthetic maytansine analogues for the targeted treatment of cancer. J Med Chem 2006;49:4392–408.
16. Lapusan S, Vidriales MB, Thomas X, de Botton S, Vekhoff A, Tang R, et al. Phase I studies of AVE9633, an anti-CD33 antibody-maytansinoid conjugate, in adult patients with relapsed/refractory acute myeloid leukemia. Invest New Drugs 2012;30:1121–31.
17. Miller ML, Fishkin NE, Li W, Whiteman KR, Kovtun Y, Reid EE, et al. A new class of antibody-drug conjugates with potent DNA alkylating activity. Mol Cancer Ther 2016;15:1870–8.
18. Broxterman HJ, Schuurhuis GJ, Lankelma J, Oberink JW, Eekman CA, Claessen AM, et al. Highly sensitive and specific detection of P-glycoprotein function for haematological and solid tumour cells using a novel nucleic acid stain. Br J Cancer 1997;76:1029–34.
19. Kovtun YV, Audette CA, Mayo MF, Jones GE, Doherty H, Maloney EK, et al. Antibody-maytansinoid conjugates designed to bypass multidrug resistance. Cancer Res 2010;70:2528–37.
20. Kondo N, Takahashi A, Ono K, Ohnishi T. DNA damage induced by alkylating agents and repair pathways. J Nucleic Acids 2010;2010:543531.
21. Loganzo F, Sung M, Gerber HP. Mechanisms of resistance to antibody-drug conjugates. Mol Cancer Ther 2016;15:2825–34.
22. Leith CP, Kopecky KJ, Chen IM, Eijdems L, Slovak ML, McConnell TS, et al. Frequency and clinical significance of the expression of the multidrug resistance proteins MDR1/P-glycoprotein, MRP1, and LRP in acute myeloid leukemia: a Southwest Oncology Group Study. Blood 1999;94:1086–99.
23. Benderra Z, Faussat AM, Sayada L, Perrot JY, Tang R, Chaoui D, et al. MRP3, BCRP, and P-glycoprotein activities are prognostic factors in adult acute myeloid leukemia. Clin Cancer Res 2005;11:7764–72.
24. Tang R, Cohen S, Perrot JY, Faussat AM, Zuany-Amorim C, Marjanovic Z, et al. P-gp activity is a critical resistance factor against AVE9633 and DM4 cytotoxicity in leukaemia cell lines, but not a major mechanism of chemoresistance in cells from acute myeloid leukaemia patients. BMC Cancer 2009;9:199.
25. Naito K, Takeshita A, Shigeno K, Nakamura S, Fujisawa S, Shinjo K, et al. Calicheamicin-conjugated humanized anti-CD33 monoclonal antibody (gemtuzumab zogamicin, CMA-676) shows cytocidal effect on CD33-positive leukemia cell lines, but is inactive on P-glycoprotein-expressing sublines. Leukemia 2000;14:1436–43.
26. Matsui H, Takeshita A, Naito K, Shinjo K, Shigeno K, Maekawa M, et al. Reduced effect of gemtuzumab ozogamicin (CMA-676) on P-glycoprotein and/or CD34-positive leukemia cells and its restoration by multidrug resistance modifiers. Leukemia 2002;16:813–9.
27. Walter RB, Raden BW, Hong TC, Flowers DA, Bernstein ID, Linenberger ML. Multidrug resistance protein attenuates gemtuzumab ozogamicin-induced cytotoxicity in acute myeloid leukemia cells. Blood 2003;102:1466–73.
28. Kung Sutherland MS, Walter RB, Jeffrey SC, Burke PJ, Yu C, Kostner H, et al. SGN-CD33A: a novel CD33-targeting antibody-drug conjugate using a pyrrolobenzodiazepine dimer is active in models of drug-resistant AML. Blood 2013;122:1455–63.
29. Gerratana B. Biosynthesis, synthesis, and biological activities of pyrrolobenzodiazepines. Med Res Rev 2012;32:254–93.
30. Bixby DL, Stein AS, Fathi AT, Kovacsovics TJ, Levy MY, Erba HP, et al. Vadastuximab talirine monotherapy in older patients with treatment naive CD33-positive acute myeloid leukemia (AML) Blood 2016;128:590.
31. Fathi AT, Erba HP, Lancet JE, Stein EM, Ravandi F, Faderl S, et al. Vadastuximab talirine plus hypomethylating agents: a well-tolerated regimen with high remission rate in frontline older patients with acute myeloid leukemia (AML) Blood 2016;128:591.
32. Godwin CD, McDonald GB, Walter RB. Sinusoidal obstruction syndrome following CD33-targeted therapy in acute myeloid leukemia. Blood 2017;129:2330–2.
33. Applebaum FR, Bernstein ID. Gemtuzumab ozogamicin for actute myeloid leukemia. Blood 2017;130:2373–6.

Published OnlineFirst March 27, 2018; DOI: 10.1158/1535-7163.MCT-17-1077

Molecular Cancer Therapeutics

IMGN779, a Novel CD33-Targeting Antibody–Drug Conjugate with DNA-Alkylating Activity, Exhibits Potent Antitumor Activity in Models of AML

Yelena Kovtun, Paul Noordhuis, Kathleen R. Whiteman, et al.

Mol Cancer Ther 2018;17:1271-1279. Published OnlineFirst March 27, 2018.